
The Mu3e experiment

F. Wauters^{1*} on behalf of the *Mu3e* collaboration

¹ PRISMA+ Cluster of Excellence and Institute of Nuclear Physics, Johannes Gutenberg
Universität Mainz, Germany
* fwauters@uni-mainz.de

February 10, 2021



Review of Particle Physics at PSI
doi:[10.21468/SciPostPhysProc.2](https://doi.org/10.21468/SciPostPhysProc.2)

Abstract

The *Mu3e* experiment aims for a single event sensitivity of $2 \cdot 10^{-15}$ on the charged lepton flavour violating $\mu^+ \rightarrow e^+e^+e^-$ decay. The experimental apparatus, a light-weight tracker based on custom High-Voltage Monolithic Active Pixel Sensors placed in a 1 T magnetic field is currently under construction at the Paul Scherrer Institute, where it will use the full intense $10^8 \mu^+/s$ beam available. A final sensitivity of $1 \cdot 10^{-16}$ is envisioned for a phase II experiment, driving the development of a new high-intensity DC muon source.

20.1 Introduction

Searches for Charged Lepton Flavour Violation (CLFV) in muon decays are a remarkably sensitive method to search for new physics processes [1]. These decays are free from Standard Model backgrounds, and leave a relatively simple and clear signature in the experimental apparatus. In addition, intense muon beams are available at several facilities, where the relatively long-lived muons get transported from a production target to an experimental area.

The Paul Scherrer Institute (PSI) has been at the forefront of CLFV searches, with the current best limit on the $\mu^+ \rightarrow e^+\gamma$ decay channel of $4.2 \cdot 10^{-13}$ (90% CL) from the *MEG* experiment [2]. The *SINDRUM* experiment [3] set the best limit on the $\mu^+ \rightarrow e^+e^+e^-$ decay channel, and the *SINDRUM II* experiment [4] on muon conversion $\mu^- \rightarrow e^-$ on gold. A new generation of experiments pursuing these three *golden* channels, which probe for new physics in a complementary manner [5], is currently under construction, such as the *Mu2e* experiment at Fermilab, the *COMET* experiment at J-PARC, and the *MEG II* experiment at PSI. The *Mu3e* experiment aims for a 10^{-16} single-event sensitivity for the $\mu^+ \rightarrow e^+e^+e^-$ CLFV decay channel, an improvement by four orders of magnitude compared to the limit set by the *SINDRUM* experiment [3]. A first phase of the experiment is currently under construction at the $\pi E5$ beamline at PSI, where the intense DC surface muon beam of $10^8 \mu^+/s$ will be exploited to achieve a single event sensitivity of $2 \cdot 10^{-15}$ in 300 days of data taking [6].

The *Mu3e* detector is optimized for the $\mu^+ \rightarrow e^+e^+e^-$ decay. It is designed to track the two positrons and one electron from muons decaying at rest with a light-weight tracker placed inside a 1 T magnetic field. The dominating accidental background originates from two ordinary muon decays where one of the positrons produces an additional electron through Bhabha scattering. This process is sufficiently suppressed by means of a good vertex resolution of better than $300 \mu\text{m}$, a timing resolution of a few 100 ps, the requirement of an invariant mass equal to the muon mass, and a balanced momentum budget. The background from $\mu^+ \rightarrow e^+e^+e^- \nu_e \bar{\nu}_\mu$ internal conversion decays can only be suppressed by means of an excellent momentum resolution of $\sigma_p < 1 \text{ MeV}$ (see Figure 20.1).

42 All *Mu3e* detector sub-systems, as described in Section 20.2, are currently under construc-
 43 tion. With the solenoid magnet (Figure 20.2) installed at PSI, the first engineering runs are
 44 planned for spring 2021.

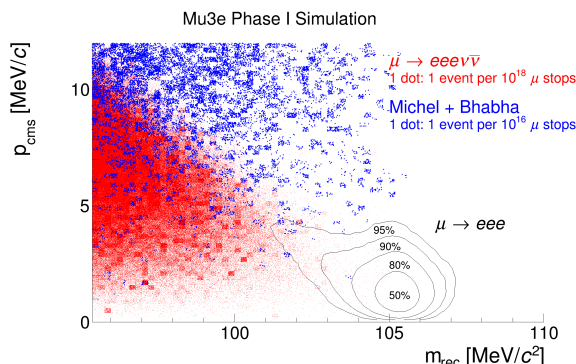


Figure 20.1: The simulated reconstructed mass versus the momentum balance of two positrons and one electron from a common vertex [6]. The accidental background is shown in blue, the dominating background from internal conversion is shown in red.



Figure 20.2: The 30 ton *Mu3e* magnet arriving at PSI. The magnet is currently installed and commissioned in the π E5 experimental area, providing a magnetic field of up to 2.6 Tesla with a $\frac{\Delta B}{B}$ uniformity and stability of $\mathcal{O}(10^{-4})$.

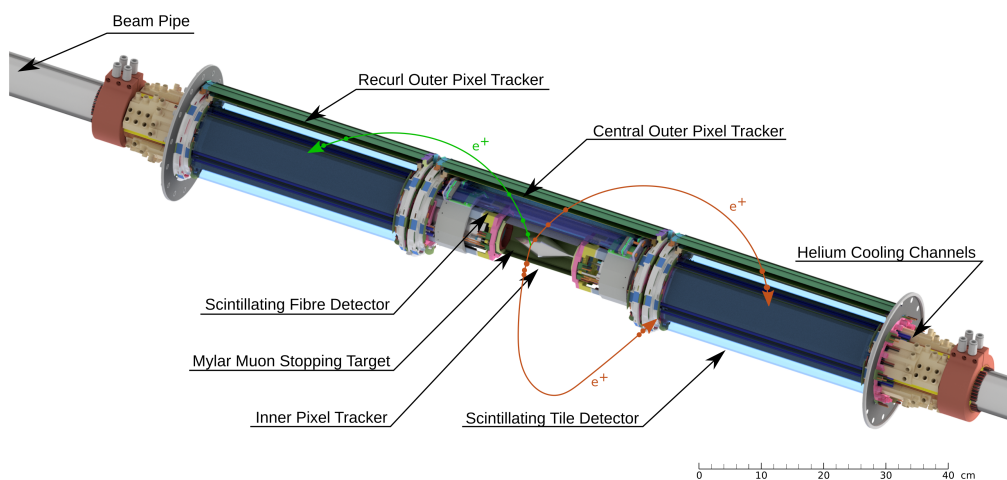


Figure 20.3: The active part of the *Mu3e* detector, with a central tracker surrounding the target, and upstream and downstream tracking stations. The large lever arm created by the recurling tracks enables the high momentum resolution required.

45 20.2 The *Mu3e* detector

46 The *Mu3e* detector is located at the Compact Muon Beam Line at the π E5 channel. After the
 47 positron contamination from the beam is removed by a Wien filter, the surface μ^+ beam of
 48 up to $10^8 \mu^+/s$ is transported to the center of the *Mu3e* solenoid magnet, and stopped on
 49 a hollow double-cone target, which spreads out the decay vertices in z and minimises the
 50 amount of target material traversed by the decay particles. The target is surrounded by the
 51 cylindrical central tracker, consisting of the inner silicon pixel detector, a scintillating fibre

52 tracker for timing purposes, and the outer silicon pixel detector. A momentum resolution of
53 better than 1 MeV/c is achieved by letting the positrons(electrons) recurl in the magnetic field,
54 either crossing the central tracker again, or hitting the outer tracking stations surrounding the
55 upstream and downstream beam pipe. These stations consist of a silicon pixel tracker, and
56 a scintillating tile detector mounted on the inside of the pixel tracker. The 5 mm thick tiles
57 enable a time resolution for the tracks reaching these outer stations of better than 100 ps. The
58 active part of the *Mu3e* detector is depicted in Figure 20.3.

59 As multiple Coulomb scattering is the dominating factor affecting the momentum resolu-
60 tion, it is crucial to minimize the material budget in the tracking detectors. For this purpose,
61 the collaboration has developed a custom High-Voltage Monolithic Active Pixel Sensor [7] (HV-
62 MAPS) based on a commercial 180 nm HV-CMOS process. After a series of prototypes showed
63 good efficiency (>99%) and time resolution ($\mathcal{O}(10\text{ ns})$) [8] [9], the current version, *MuPix10*
64 (Figure 20.4), is a full sized $2\times 2\text{ cm}^2$ sensor with $80\times 80\text{ }\mu\text{m}^2$ active pixels which is thinned
65 to $50\text{ }\mu\text{m}$. The digital periphery provides up to three 1.25 Gbit/s Low-Voltage Differential
66 Signaling (LVDS) continuous data connections to the front-end electronics. The sensors are
67 bonded to a thin aluminum/polyimide flex print carrying all electrical signals. Together with
68 a polyimide support structure, the entire silicon tracking module has a thickness of ca. 0.0012
69 radiation lengths. The pixel sensors generate about 250 mW/cm^2 of heat. To remove this
70 heat whilst keeping the material budget of the tracker sufficiently low, a gaseous He cooling
71 system [10] is deployed providing well controlled He flows at atmospheric pressure between
72 and outside the pixel layers.

73 A time resolution of about 10 ns is insufficient to determine the direction and thus the
74 charge of the decay particles. A scintillating fibre detector is therefore placed between the
75 inner and outer layer of the central silicon-pixel tracker, consisting of a dozen 30 cm long rib-
76 bons made from three staggered layers of $250\text{ }\mu\text{m}$ diameter multicladd round fibers, read out
77 by SiPM arrays on both sides [11]. Located at the very end of the recurling particle trajectories
78 hitting the upstream or downstream tracker, where the constraints on the material budget are
79 less stringent, the tile detector provides the needed precise timing information of the particle
80 tracks, in conjunction with the fibre detector significantly reducing the combinatorial back-
81 ground associated with the intense rate of $10^8\text{ }\mu^+/\text{s}$. Each of the 5824 individually wrapped
82 tiles is read out by a single SiPM. Both the fibre and tile SIPM signals are processed by a cus-
83 tom Application-Specific Integrated Circuit (ASIC), the 32 channel *MuTrig* chip [12], which
84 applies 2 thresholds to the analogue signal for time and energy information. The *MuTrig* chip
85 has a 1.25 Gbit/s LVDS data connection, similar to the *MuPix* chip readout. For tile and fibre
86 detector a respective time resolution of $<50\text{ ps}$ and $<400\text{ ps}$ is achieved.

87 The entire *Mu3e* detector is mounted in the bore of a superconducting magnet. Figure 20.2
88 shows the 3 m long solenoid magnet with the iron return yoke. It has a 1 m wide bore housing
89 the active detector, in addition to the support structures and services such as the front-end
90 readout electronics and DC-DC power converters for the detector ASICs. The two flanges
91 below and above the beam pipe provide access for the water and gaseous helium cooling
92 pipes, the power cables, and the optical data connections.

93 20.3 Readout and online event selection

94 With three lepton tracks going in different (opposite) directions, the topology of a $\mu^+ \rightarrow e^+e^+e^-$
95 event is such, that a global picture of the detector is needed before candidate events can be
96 selected. This leads to a trigger-less readout scheme as shown in Figure 20.6, where all pixel,
97 fibre and tile hits are continuously being digitized and merged into a data stream of up to 100
98 Gbit/s. A series of PCs housing powerful Graphics Processing Units (GPU) perform an online
99 event-selection, reducing the data rate to a manageable 50-100 MByte/s which is stored for
100 further offline processing.

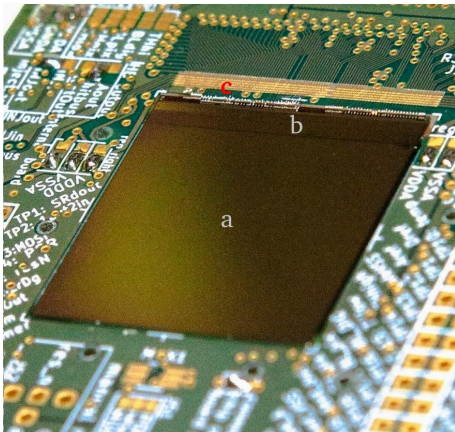


Figure 20.4: The full sized MuPix sensor, with a) a $2 \times 2 \text{ cm}^2$ sized active area, and b) a periphery with the pixel hit digitization and read-out state machine. This chip is c) wire bonded to a PCB for testing purposes.

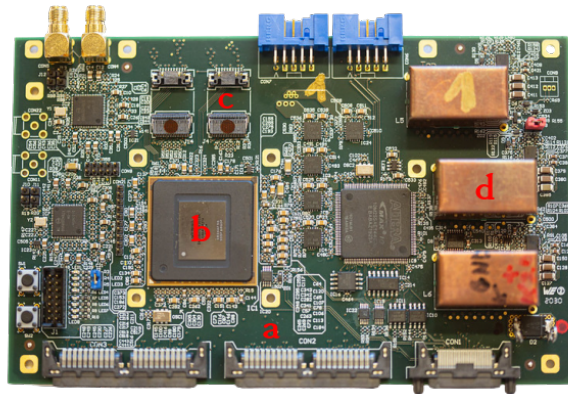


Figure 20.5: The front-end readout board, combining and time sorting the a) data from up to 36 detector ASICs on b) an Arria V FPGA, before sending the data via the c) optical Samtec FireFly transceivers. d) Custom DC-DC converters with air coils regulate the power on the board.

101 Each detector ASIC, a *MuTrig* or *MuPix* chip, assigns a timestamp and address to each hit,
 102 and sends the serialized data through a series of flex-prints and twisted pair cables to a front-
 103 end board (Figure 20.5). Each of these readout boards is located inside the magnet bore and
 104 accepts up to 45 electric LVDS links. The data streams are merged and time-sorted on an Arria V
 105 Field-Programmable Gate Array (FPGA). Two optical transceivers provide eight 6 GBit/s links
 106 to the outside, sending off the merged and sorted hit information combined with the slow-
 107 control data. In addition, the front-end FPGA also configures the detector ASICs, including
 108 tuning the very large number of individual *MuPix* pixels, and distributes the clock and reset
 109 signals.

110 All incoming and outgoing data connections to and from the detector volume travel via
 111 optical fibres to the counting house. The data links from the 112 front-end boards are con-
 112 nected to the *Switching boards*, where the data from different detector modules are merged
 113 into 64 ns time slices containing the full detector hit information. This custom *PCIe40* board
 114 housing a large Arria 10 FPGA and 48 fast optical receivers and 48 fast optical transmitters
 115 was developed for the LHCb and ALICE upgrades [13].

116 The online event selection must decide which of these 64 ns *snapshots* of the detector to
 117 store for later (offline) processing, in the process keeping less than 1% of the data. A simple
 118 time coincidence between 3 tracks is insufficient to achieve this. Instead an online filter farm
 119 reconstructs all tracks in software, and performs the selection by requiring 3 tracks having a
 120 common vertex and the kinematics of a possible $\mu^+ \rightarrow e^+e^+e^-$ event. The filter farm consists of
 121 12 PC's housing a FPGA board receiving the data and a powerful commercial GPU performing
 122 the event selection. With simple geometric cuts, candidate tracks are first selected on the
 123 FPGA from hits in the central pixel tracker. The track fitting [14] is performed on the GPU,
 124 where $1 \cdot 10^9$ fits per second were achieved on a NVIDIA GTX 980 GPU, sufficient to be able to
 125 process the expected 10^8 muon decays/s. A newer more powerful GPU will be selected when
 126 equipping the farm PCs.

127 The MIDAS¹-based data-acquisition system sends the filtered data to on-site and off-site
 128 storage for later processing. This integrated DAQ also takes care of the configuration, mon-

¹<https://midas.triumf.ca>

129 itoring, and logging of all parameters of the detector and its services such as the water and
 130 helium cooling system and power distribution.

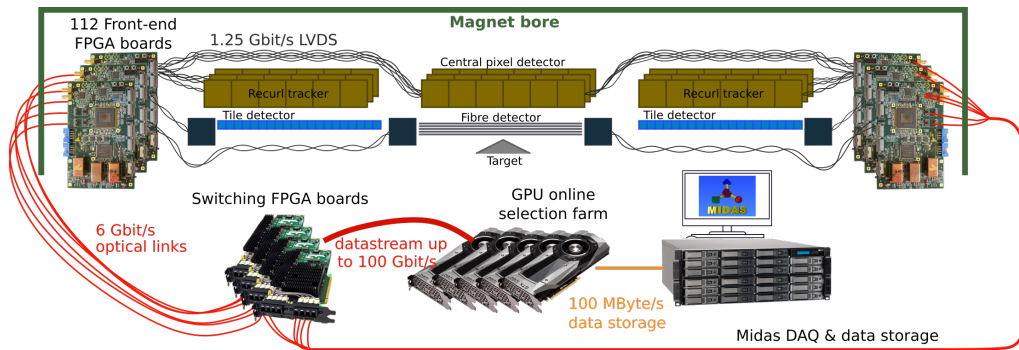


Figure 20.6: A sketch of the *Mu3e* triggerless readout scheme, where all detector hits are piped to the online filter farm. A selection algorithm based on massive parallelised track fitting sends off a subset of the data for further offline processing.

131 20.4 Conclusions and outlook

132 With the magnet installed at the Paul Scherrer Institute, the *Mu3e* experiment is entering
 133 its construction phase. All sub-detector demonstrators have met the required specification,
 134 and are currently being integrated to a single lightweight electron/positron tracker. This also
 135 includes a novel read-out system of the apparatus, which pipes the full detector information to
 136 an online filter farm. Aside from being a necessary requirement set by the CLFV decay event
 137 topology, this readout scheme where the full and global detector information is available for
 138 online analysis, also allows other new-physics searches such as CLFV two-body decays and
 139 Dark Photon searches [15].

140 The *Mu3e* phase II experiment envisions a sensitivity of $1 \cdot 10^{-16}$. Many detector sub-
 141 systems are already designed with this goal in mind, but significant research and development
 142 on the detector side still has to be done. Such an order of magnitude increase in sensitivity
 143 also requires a more intense, and currently unavailable muon flux of μ^+ /s of $\mathcal{O}(10^9)$. For this
 144 purpose, a new High-Intensity Muon Beamline [16] to be installed at the target M is currently
 145 under development at the Paul Scherrer Institute, replacing the conventional muon extraction
 146 beamline elements with solenoids. The timeline of this project coincides with the envisioned
 147 start of the *Mu3e* Phase II construction at the end of this decade.

148 References

- 149 [1] Y. Kuno and Y. Okada, *Muon decay and physics beyond the standard model*, Rev. Mod.
 150 Phys. **73**, 151 (2001), doi:[10.1103/RevModPhys.73.151](https://doi.org/10.1103/RevModPhys.73.151), [hep-ph/9909265](https://arxiv.org/abs/hep-ph/9909265).
- 151 [2] A. Baldini *et al.*, *Search for the lepton flavour violating decay $\mu^+ \rightarrow e^+ \gamma$ with the full dataset
 152 of the MEG experiment*, Eur. Phys. J. C **76**(8), 434 (2016), doi:[10.1140/epjc/s10052-
 153 016-4271-x](https://doi.org/10.1140/epjc/s10052-016-4271-x), [1605.05081](https://arxiv.org/abs/1605.05081).
- 154 [3] U. Bellgardt *et al.*, *Search for the Decay $\mu^+ \rightarrow e^+ e^+ e^-$* , Nucl. Phys. B **299**, 1 (1988),
 155 doi:[10.1016/0550-3213\(88\)90462-2](https://doi.org/10.1016/0550-3213(88)90462-2).

- 156 [4] W. H. Bertl *et al.*, *A Search for muon to electron conversion in muonic gold*, Eur. Phys. J. C
157 **47**, 337 (2006), doi:[10.1140/epjc/s2006-02582-x](https://doi.org/10.1140/epjc/s2006-02582-x).
- 158 [5] A. Crivellin, S. Davidson, G. M. Pruna and A. Signer, *Renormalisation-group improved*
159 *analysis of $\mu \rightarrow e$ processes in a systematic effective-field-theory approach*, JHEP **05**, 117
160 (2017), doi:[10.1007/JHEP05\(2017\)117](https://doi.org/10.1007/JHEP05(2017)117), [1702.03020](https://arxiv.org/abs/1702.03020).
- 161 [6] K. Arndt *et al.*, *Technical design of the phase I Mu3e experiment*, arXiv:2009.11690 (2020),
162 [2009.11690](https://arxiv.org/abs/2009.11690).
- 163 [7] I. Peric, *A novel monolithic pixelated particle detector implemented in high-voltage CMOS*
164 *technology*, Nucl. Instrum. Meth. A **582**, 876 (2007), doi:[10.1016/j.nima.2007.07.115](https://doi.org/10.1016/j.nima.2007.07.115).
- 165 [8] H. Augustin *et al.*, *Performance of the large scale HV-CMOS pixel sensor MuPix8*, JINST
166 **14**(10), C10011 (2019), doi:[10.1088/1748-0221/14/10/C10011](https://doi.org/10.1088/1748-0221/14/10/C10011), [1905.09309](https://arxiv.org/abs/1905.09309).
- 167 [9] H. Augustin *et al.*, *The MuPix System-on-Chip for the Mu3e Experiment*, Nucl. Instrum.
168 Meth. A **845**, 194 (2017), doi:[10.1016/j.nima.2016.06.095](https://doi.org/10.1016/j.nima.2016.06.095), [1603.08751](https://arxiv.org/abs/1603.08751).
- 169 [10] F. Meier Aeschbacher, M. Deflorin and L. O. S. Noehte, *Mechanics, readout and cooling sys-*
170 *tems of the Mu3e experiment*, In *28th International Workshop on Vertex Detectors* (2020),
171 [2003.11077](https://arxiv.org/abs/2003.11077).
- 172 [11] A. Bravar, K. Briggel, S. Corrodi, A. Damyanova, L. Gerritzen, C. Grab, M. Hildebrandt,
173 A. Papa and G. Rutar, *The Mu3e scintillating fiber timing detector*, Nucl. Instrum. Meth.
174 A **958**, 162564 (2020), doi:[10.1016/j.nima.2019.162564](https://doi.org/10.1016/j.nima.2019.162564).
- 175 [12] H. Chen, K. Briggel, P. Eckert, T. Harion, Y. Munwes, W. Shen, V. Stankova and H. Schultz-
176 Coulon, *MuTRiG: a mixed signal Silicon Photomultiplier readout ASIC with high timing*
177 *resolution and gigabit data link*, JINST **12**(01), C01043 (2017), doi:[10.1088/1748-](https://doi.org/10.1088/1748-0221/12/01/C01043)
178 [0221/12/01/C01043](https://doi.org/10.1088/1748-0221/12/01/C01043).
- 179 [13] P. Durante, N. Neufeld, R. Schwemmer, U. Marconi, G. Balbi and I. Lax, *100 Gbps*
180 *PCI-Express Readout for the LHCb Upgrade*, IEEE Trans. Nucl. Sci. **62**(4), 1752 (2015),
181 doi:[10.1109/TNS.2015.2441633](https://doi.org/10.1109/TNS.2015.2441633).
- 182 [14] A. Kozlinskiy, A. Schöning, M. Kiehn, N. Berger and S. Schenk, *A new track reconstruction*
183 *algorithm for the Mu3e experiment based on a fast multiple scattering fit*, JINST **9**(12),
184 C12012 (2014), doi:[10.1088/1748-0221/9/12/C12012](https://doi.org/10.1088/1748-0221/9/12/C12012).
- 185 [15] A.-K. Perrevoort, *The Rare and Forbidden: Testing Physics Beyond the Standard Model*
186 *with Mu3e*, SciPost Phys. Proc. **1**, 052 (2019), doi:[10.21468/SciPostPhysProc.1.052](https://doi.org/10.21468/SciPostPhysProc.1.052),
187 [1812.00741](https://arxiv.org/abs/1812.00741).
- 188 [16] R. Iwai *et al.*, *Development of next generation muon beams at the Paul Scherrer Institute*,
189 PoS **NuFact2019**, 125 (2020), doi:[10.22323/1.369.0125](https://doi.org/10.22323/1.369.0125).